WELDING RESEARCH

SUPPLEMENT TO THE *WELDING JOURNAL*, MAY 2018
Sponsored by the American Welding Society

Influence of Horn Misalignment on Weld Quality in Ultrasonic Welding of Carbon Fiber/Polyamide 66 Composite

Experiments showed horn misalignment of more than 4 deg resulted in a significant decrease in weld area, weld strength, and cosmetic quality

BY Q. ZHI, L. LU, Z.-X. LIU, AND P.-C. WANG

ABSTRACT

In this study, the influence of horn axial misalignment on the quality of ultrasonic welded lapped carbon-fiber/polyamide 66 composite (C_f /PA 66) was investigated. An analytical model was derived to estimate the energy absorption in the welding zone of the thermoplastic material and, consequently, permit the estimation of weld size. Using this model, the effect of the horn misalignment on the weld size was examined and validated. Results of the modeling and experiments showed the horn misaligned by more than 4 deg resulted in a significant decrease in weld area, weld strength, and cosmetic quality, which was mainly attributed to the energy deviation at the faying surfaces. This study provides a good understanding of the influence of horn misalignment on the quasi-static characteristics of the ultrasonic welded carbon-fiber-reinforced polyamide 66 composite.

KEYWORDS

• Carbon-Fiber/Polyamide 66 Composite • Ultrasonic Welding
• Horn Misalignment • Weld Strength

Introduction

Carbon-fiber-reinforced thermoplastics (CFRTP) have received much attention recently due to their high strength/elasticity-to-weight ratios, as well as high damping capability compared to metallic materials (Refs. 1–5). To expand the application of CFRTP, joining of CFRTP to form large and complex engineering structures is inevitable. Joining methods ranging from conventional adhesive bonding and mechanical fastening to new welding techniques, such as ultrasonic welding (Ref. 6) and laser welding (Ref. 7), were developed. Among these joining methods, ultrasonic welding seems most promising because it is fast (Refs. 8, 9), energy efficient (Refs. 10, 11), and easy to automate for mass production (Refs. 2, 12).

The essence of ultrasonic welding of polymers is to form a weld at the contact site of the surface between the two welded workpieces. Referring to Fig. 1A, the mechanical vibration passes through the horn to the workpieces. The intermolecular friction and dissipated energy at the contact site of the workpieces heat the contact surface up to or above the melting point of the thermoplastic. As the process proceeds, the contact site, which usually consists of the surface and/or fabricated asperities, is melted and grows until the vibration stops. Consequently, the reliable contact between the horn and the workpiece under the horn pressure is extremely important because it affects the ultrasonic wave transmission and energy conversion (Refs. 13–15). Although it is critical to maintain intimate contact between the horn and workpiece, it is conceivable that horn-to-workpiece misalignment may occur because the workpieces may have variations in geometry and dimensions resulting from compression, injection molding, and clamping, which would affect the quality of the welds. Under service loading conditions, the misaligned weld may induce greater stress concentrations and, therefore, degrade the joint performance. Thus, it is essential that an understanding of the influence of horn misalignment on the quality of the ultrasonic welded carbon-fiber composite be obtained.

To further understand the ultrasonic welding process, a method in view of ultrasonic wave propagation in materials had been proposed by some researchers (Refs. 16–18). They discovered the propagation of ultrasonic waves in materials accompanied the wave reflecting, transmitting, and absorbing by the materials and interfaces of materials, indicating the intensity of the ultrasonic energy attenuated during its propagation.

https://doi.org/10.29391/2018.97.012

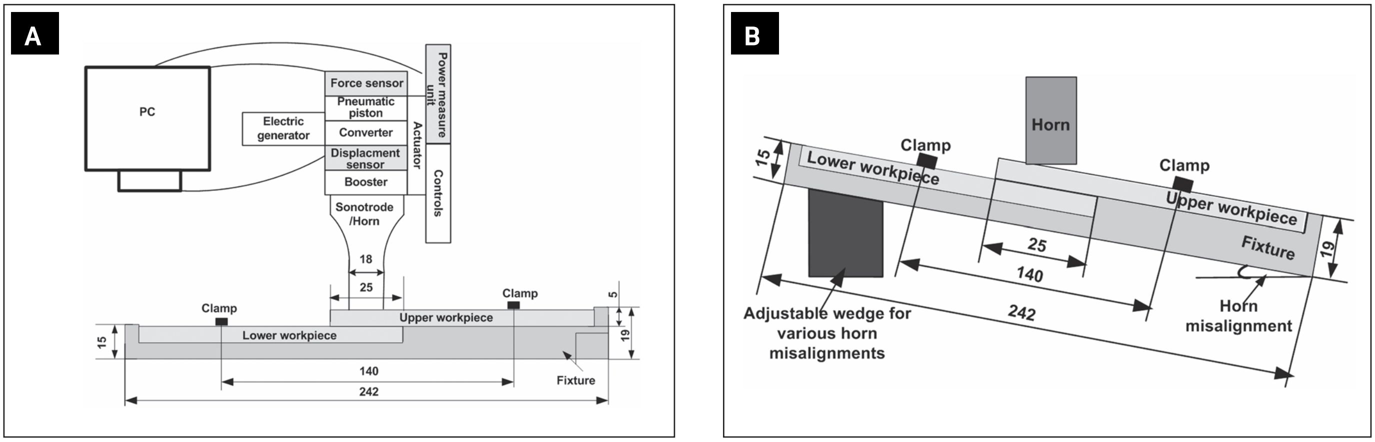

Fig. 1 — Schematic of ultrasonic welding: A — Normal configuration; B — with horn-to-workpiece misalignment (dimensions: mm).

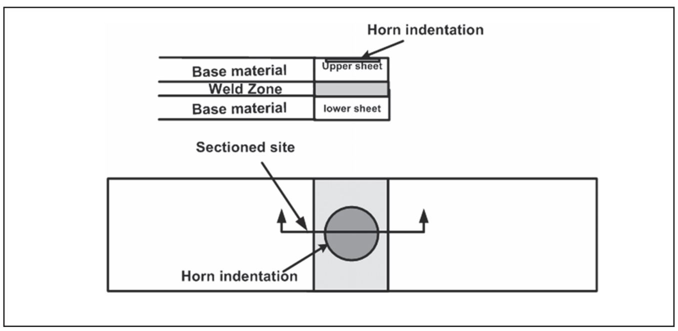

Fig. 2 — Schematic of sample preparation for examining the microstructure of the ultrasonic welded 4-mm- (0.16-in.-) thick injection molded C_f/PA 66 composite.

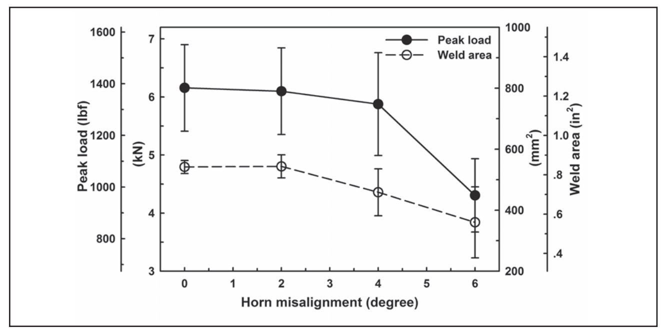

Fig. 3 — Effect of horn axial misalignment on the strength and weld area of the ultrasonic welded 4-mm- (0.16-in-) thick lap C_f/PA 66 composite with 30 wt-% fiber.

In addition, Khmelev et al. (Ref. 18) estimated the energy in a weld zone with the wave propagation method and found a criterion for the formation of a quality weld. However, this study (Ref. 18) assumed there was reflecting and transmitting on an interface of medium, and neglected the absorption by the surface of the material. Moreover, the contact between the welding horn and workpieces was intimate in Khmelev's work.

The present study was undertaken to evaluate the effect of horn axial misalignment on the quality of ultrasonic welded lapped carbon-fiber/polyamide 66 composite (C_f/PA 66). A model based on the work of Khmelev et al. (Ref. 18) is proposed to analyze the influence of horn misalignment on ultrasonic wave propagation. Ultrasonic welded lapped carbon-fiber/polyamide 66 (C_f/PA 66) composite joints with 30 wt-% fiber without an energy director, shown in Fig. 1B, were made with various horn misalignments encountered by the ultrasonic welded carbon-fiber thermoplastic components. The influence of horn axial misalignment on the strength, microstructure, fracture mode, and cosmetic quality of the welds was studied. This study provides a good understanding of the effect of horn misalignment on the quasi-static characteristics of the ultrasonic welded carbon-fiber polyamide 66 composite.

Experimental Procedure

Injection Molded Carbon-Fiber Composite

Commercial polyamide 66 and carbon fiber (24K, T300 type, Toray Carbon Magic Co. Ltd.) with a length of 2 mm (0.08 in.) and a diameter of 7 µm (2.8×10^{-4} in.) were selected in this study. The fibers were first cleaned with a concentrated solution of nitric acid and then surface pretreated with 8% diglycidyl ether of bisphenol solution in acetone. Both polyamide 66 and pretreated carbon fibers were dried at 80°C (176°F) in a vacuum condition for 3 h before being used to fabricate C_f/PA 66 composite with 30 wt-% fiber.

A twin-screw extruder with two separate inlets was used to mold C_f/PA 66 composite. Polyamide 66 was added to the first hopper, and carbon fibers were added to the second hopper. Polyamide 66 was fully melted before carbon fibers were added to minimize the fracture of the carbon fiber during compounding. The processing temperature was within 270°–280°C (518~536°F), and the screw speed was 180 rpm. After fully mixing polyamide 66 with carbon fibers in a twin-screw extruder, the C_f/PA 66 composite was processed into 2-mm-long (0.08-in.-long) pellets. The pellets were then fed into the injection extruder to mold into coupons with dimensions of $132 \times 38 \times 4.0$ mm ($5.2 \times 1.5 \times 0.16$ in.). All coupons were stored in an ambient laboratory environment (i.e., 20°C and 50% R.H.) and dried in an oven at 80°C (176°F) for 48 h before welding to remove moisture in the specimens. The injection molded carbon-fiber/polyamide 66 composite exhibited a tensile strength of 99.2 ± 3 MPa [$(1.4 \pm 0.4) \times 104$ lb/in.^{2}] and an elastic modu-

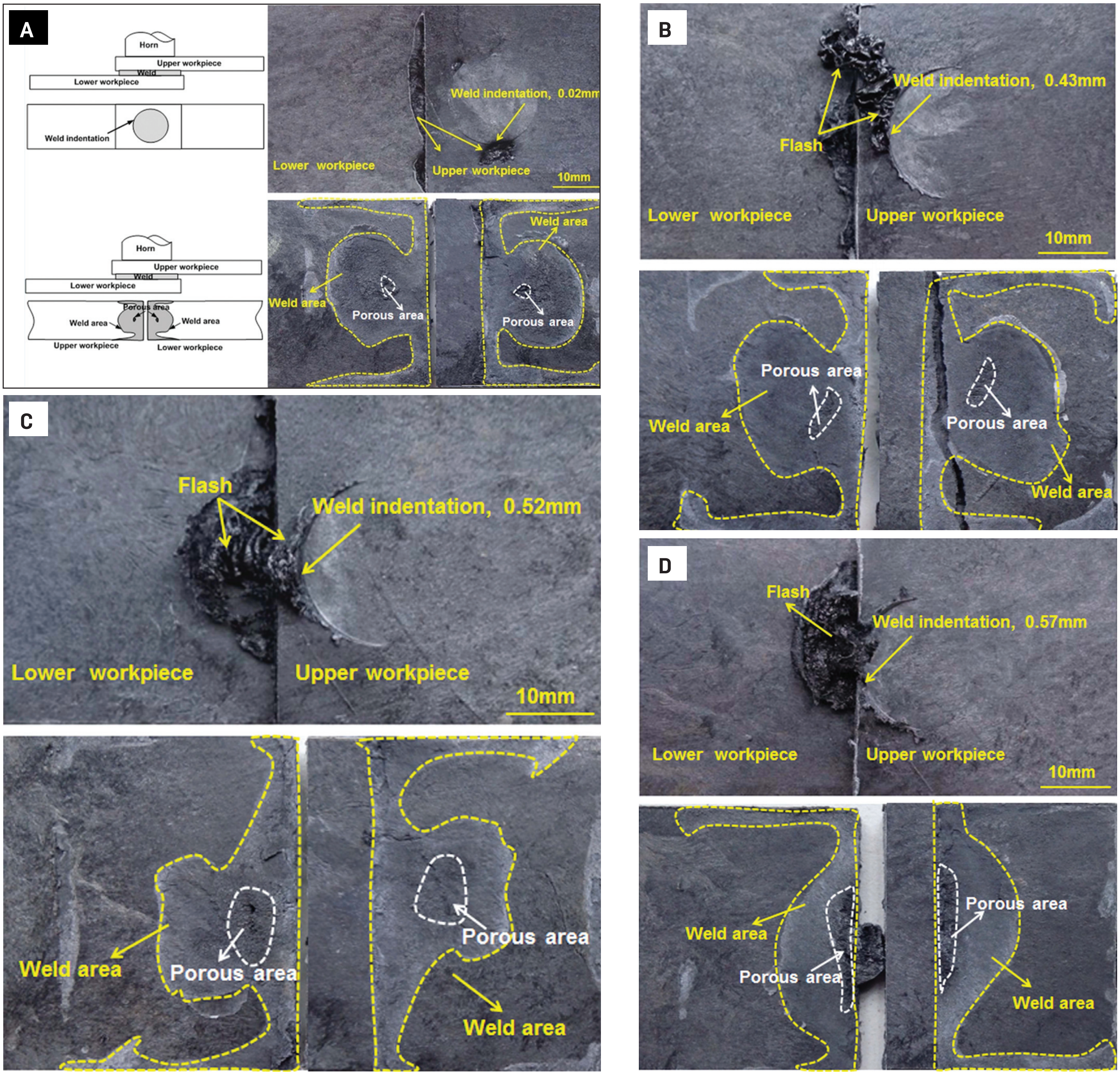

Fig. 4 — Effect of horn axial misalignment on the weld indentation and weld area of the ultrasonic welded 4-mm- (0.16-in.-) thick C_f/PA 66 composite: A — 0; B — 2; C — 4; D — 6 deg.

lus of 8936 ± 3 MPa [(1.3 ± 0.6) × 106 lb/in.^{2}], respectively.

Ultrasonic Welding

The ultrasonic welding process was performed using a KZH-2026 multifunction ultrasonic welding (UW) machine (Kaizheng Ultrasonic Technologies Co. Ltd., Weihai, China) with a nominal power of 2.6 kW, nominal frequency of 20 kHz, and nominal amplitude of 25 μm (9.8×10^{-4} in.). The machine was equipped with a data acquisition system that combined with pressure, horn-displacement, and time sensors, which were integrated in the controller of the UW machine. In addition, the weld force, weld energy, and displacement of the horn were recorded online in a PC as a function of time by the data acquisition system. The final horn displacement, weld energy, weld time, weld force, hold time, and delay time were also displayed in the control panel during the UW process. To avoid coupon motion during welding, the coupons were held in place using a fixture.

The machine had three welding modes: energy, time, and collapse modes. The value of weld energy, weld time, and horn displacement for the three modes, respectively, were preset to control the welding process. The workpieces were then welded us-

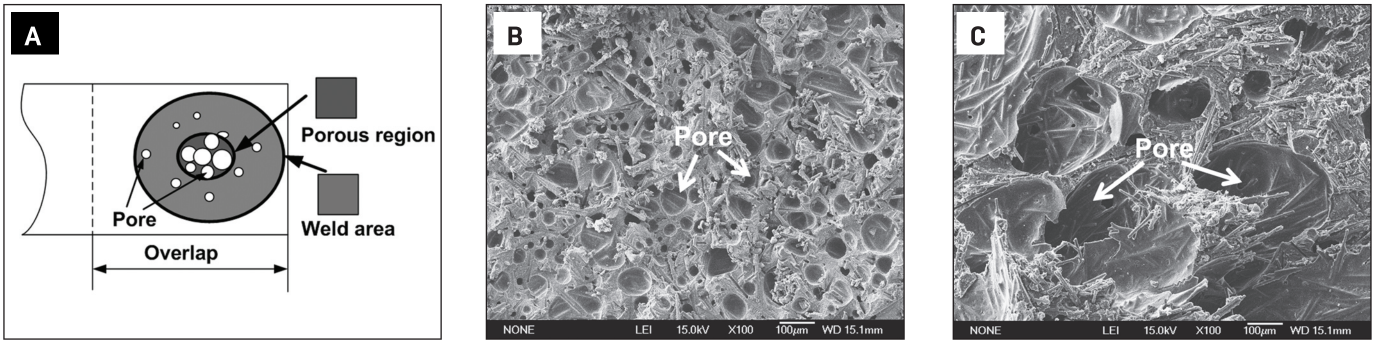

Fig. 5 — A — Schematic of the weld area and porous region; B — typical microstructures of pores in weld area; C — in porous region of the joint made with a 2-deg horn misalignment.

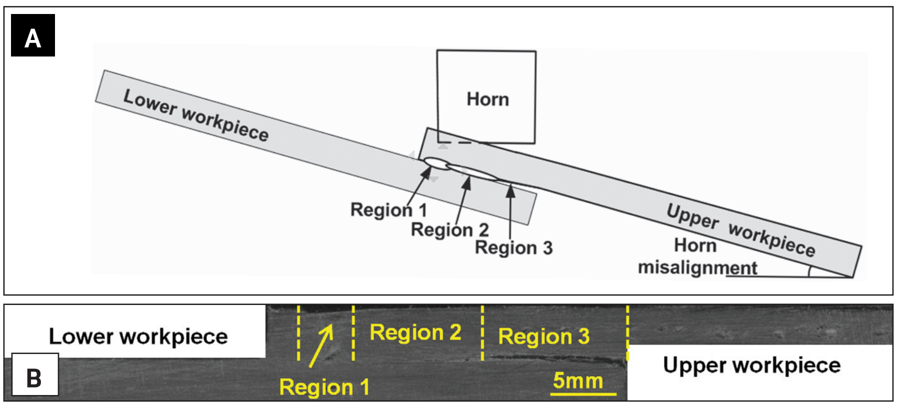

Fig. 6 — A — Schematic of ultrasonic welding with a horn misalignment; B — cross section of a weld made with a horn axial misalignment.

ing nominal power of the machine. When the weld energy, weld time, or horn displacement reached the preset values for the selected weld mode, ultrasonic wave oscillation was stopped. Therefore, weld quality was controlled by the preset values in each selected welding mode. When time/energy mode was selected, the values of the delay time, weld force, hold time, and weld time/energy were preset prior to welding. When ultrasonic triggering was performed, the horn was pressed onto the workpieces for 2 s, and then ultrasonically vibrated until the preset energy was reached. All specimens were welded using a 7075 aluminum horn with a diameter of 18 mm (0.71 in.).

Weld Microstructure

To assess the microstructure characteristics of the ultrasonic welded joints, the specimens were prepared using the procedures shown in Fig. 2 for the tested joints. The joints were notched from the central position of the weld first, then, the pre-notched specimens were immersed in liquid nitrogen for 10 min. The embrittled specimens were broken off from the notched site; the broken specimens were sputter-coated with gold for 50 s to increase conductivity, and the microstructures of the welds were examined with a scanning electron microscope (JSM6700F).

Quasi-Static Test

Quasi-static tests were performed by loading each joint to fracture in an MTS 810 tensile tester per ASTM D1002-2001. To minimize bending stresses inherent in the testing of single-lap weld specimens, filler plates were attached onto both ends of the specimen using a masking tape to accommodate the sample offset. Load vs. displacement results were obtained, as the specimens were loaded at a stroke rate of 2.0 mm/min (i.e., 0.08 in./min). Weld strength was evaluated by peak load. Three replicates were performed, and the average weld strengths were reported.

Results and Discussion

Effect of Horn Axial Misalignment on Weld Strength

In the actual production of the joints, the welds were formed in a large plate of molded C_f/PA 66 composite. The procedure for welding a large plate was usually to form two welds at a relatively large distance (larger than the distance between two normal welds) first and then welded in the center of the two existing welds until the needed number of the weld for the plate was obtained. During this procedure, there may exist some deformations around the existing welds, and these deformations made the whole plate deform slightly, which may lead to the existence of horn-to-workpiece misalignment. To evaluate the influence of horn misalignment on the weld quality, ultrasonic welding with various horn off-angles was studied.

To examine the effect of horn misalignment on the quality of the ultrasonic welds, welding tests were performed with the introduction of various horn misalignments (i.e., 2, 4, and 6 deg), referring to Fig. 1B. Figure 3 presents the influence of horn misalignment on the strength and weld area of the ultrasonic welded 4.0-mm- (0.16-in.-) thick C_f/PA 66 composite fabricated with a welding time of 2.1 s and a horn pressure of 0.15 MPa (21.76 lb/in.^{2}). Referring to Fig. 3, an increase in horn misalignment led to a decrease in weld strength and weld area, which was particularly pronounced for the horn misalignment between 4 and 6 deg. Careful examination of the tested welds indicated the welding horn and

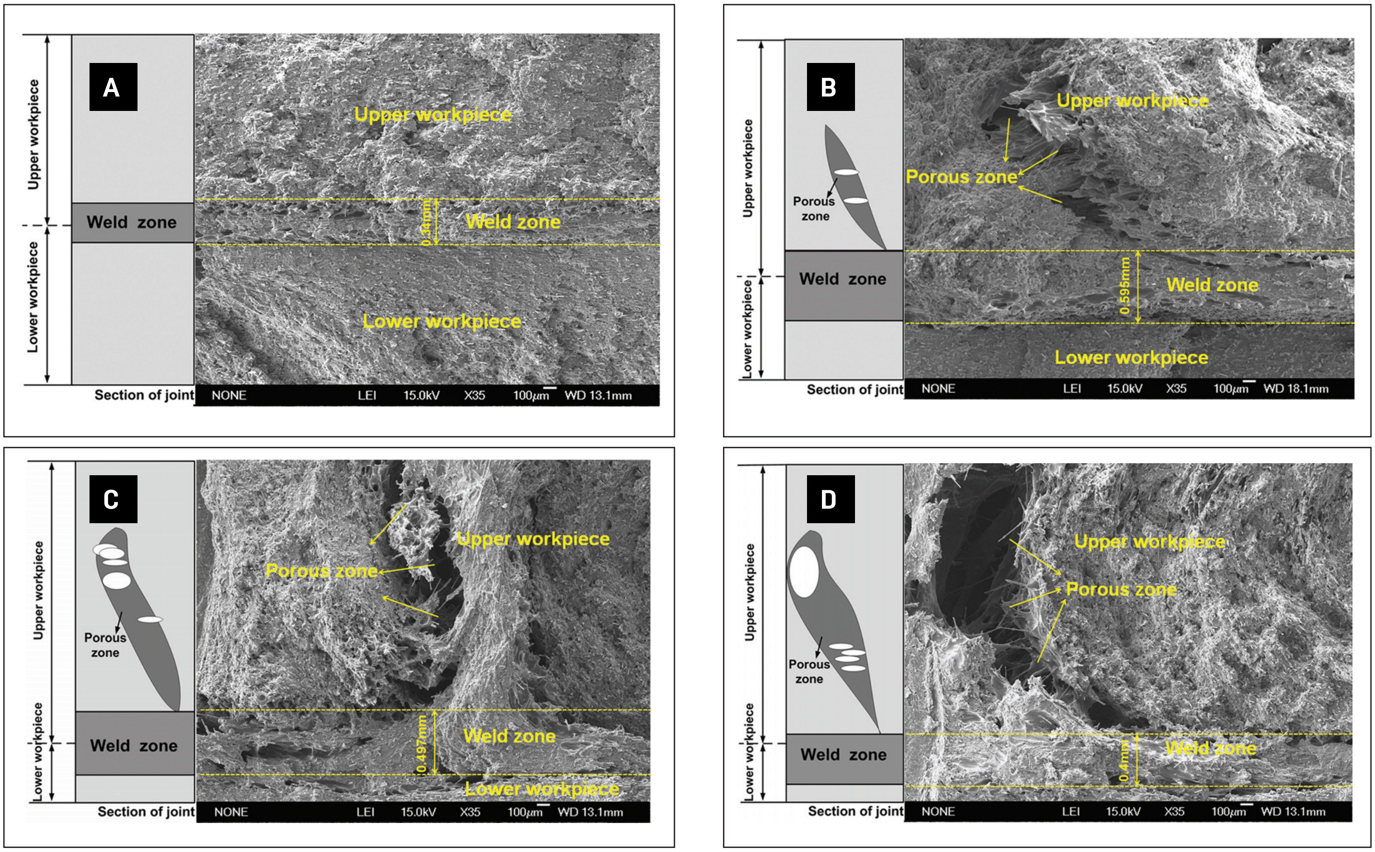

Fig. 7 — Effect of horn axial misalignment on the microstructures at region 1 of the ultrasonic welded 4-mm- (0.16-in.-) thick C_f/PA 66 composite: A — 0; B — 2; C — 4; D — 6 deg.

workpieces were not in intimate contact. It is well known that the strengths of the welds were closely correlated with the weld areas and the microstructures (Refs. 19, 20).

To further understand the influence of horn axial misalignment on the weld strength, the contact between the horn and workpiece were examined and the results are shown in Fig. 4. Referring to Fig. 4, the fracture surfaces of the welds revealed a decrease in the weld area as the horn misalignment increased. Careful examinations of the weld areas revealed the intimate contacts hardly existed at the faying surfaces due to the uneven pressure caused by the off-angled horn. The uneven pressure at the horn-workpiece interfaces resulted in the severe uneven surface indentation (especially for the horn misaligned by more than 4 deg) on the surface of the upper workpiece and the formation of pores in the weld.

Figure 5 shows the typical microstructures of the weld area and porous region observed in Fig. 4 for the weld made with a 2-deg horn misalignment. The combination of analysis results shown in Figs. 4 and 5 revealed the weld contained some small pores while rather large pores were observed at the porous region. Referring to the experimental observations, the pores increased in size and density as the horn misalignment increased. The occurrence of pores was likely from the excessive heat in the weld or the entrapped moisture in the materials (Ref. 21). Our previous studies (Refs. 22, 23) revealed the entrapped moisture in the C_f/PA 66 composite resulted in pores during ultrasonic welding. Since the workpieces were dried in a vacuum oven at 80°C for 48 h before welding (described in the section titled Injection Molded Carbon Fiber Composite), the majority of the pores observed were likely from excessive heating during welding rather than entrapped moisture.

Influence of Horn Axial Misalignment on Weld Microstructure

It was well known that the weld strength was correlated with the weld microstructures (Ref. 24). To understand how a horn misalignment affected the microstructure and strength of the welds, the welds made with a horn misalignment were cross sectioned and examined. Figure 6A, B shows schematics of ultrasonic welding with an off-angle horn and cross section of a weld made with a horn misalignment, respectively. Severe contacts developed at region 1 where the horn indented into the upper workpiece, while loose contacts developed at regions 2 and 3. Figures 7, 8, and 9 present the influence of horn misalignment on the microstructures at regions 1, 2, and 3 of the welds, respectively. As shown in Fig. 7, the porous area increased and thickness of the melt decreased as the horn misalignment increased from 0 to 6 deg. The expansion of the porous zone was likely the result of excessive heat produced at the contact site of the horn to workpiece. The reduction in melt thickness was primarily attributed to the fact the molten material was squeezed out as a result of the high pressure at region 1 of the faying surfaces. These results agreed with the observations shown in Fig. 4.

While similar results shown in Fig. 8 were observed for region 2 of the welds, hardly any weld was formed at region 3 as shown in Fig. 9. Referring to Fig. 9, the unfused zone increased with an increase in horn misalignment, which increased to 9 mm (0.35 in.) for 6 deg from 2 mm (0.08 in.) for a 2-deg horn misalignment. These results suggested the misaligned weld was the main reason for the decrease in weld strength.

Effect of Horn Misalignment on Fracture Mode

After the influence of horn misalignment on the appearances, fracture surfaces, and microstructures of the welds was investigated, the fracture modes of the welds made with various horn misalignments were examined as well. Visual examinations of the quasi-static tested welds indicated the nominal welds and welds with a smaller than 4-deg misalignment had similar fracture modes — Fig. 10A. As the horn misalignment increased, the weld area at the faying surfaces decreased, and consequently led to an interfacial fracture mode, as shown in Fig. 10B.

The results described above indicated the intimate contacts between the horn and workpiece produced welds with a uniform melt thickness, which can bear the stress evenly under the loading and, consequently, it is more likely to fracture through the workpiece. These results indicated the fracture mode of a weld was closely related to the weld size. The weld size mainly depended on the horn-to-workpiece contact under a given set of weld variables. The horn misalignment influenced ultrasonic wave transmission, and therefore it would be necessary to have a good part fitup to ensure proper contact between the horn and workpiece in ultrasonic welding.

Modeling Effect of Horn Misalignment on Ultrasonic Wave Transmission

The ultrasonic energy was continuously conducted from the horn into the workpieces in the form of ultrasonic waves until the end of the welding process. All the ultrasonic energy was dissipated by the workpieces and interfaces during the propagation process. To assess the influence of horn misalignment on weld quality, a model based on the work of Khmelev et al. (Ref. 18) was formulated. Figure 11 shows the schematic of the ultrasonic welding process where the upper and lower workpieces are perpendicular to a horn and supported by an anvil. During ultrasonic welding, the ultrasonic energy in the form of ultrasonic waves propagate from the horn to the workpieces and bounce back to the horn and top surface of the upper workpiece (i.e., interface I), which are defined as the first cycle. The ultrasonic waves are attenuated during the traveling, and the remaining ultrasonic waves are propagated to the workpieces and reflected to interface I, which are treated as the second cycle. Similar behavior continues and is designated as the third, fourth, and fifth cycles and so forth. This process continues until all ultrasonic energy is dissipated completely.

With the presence of a horn misalignment (Fig. 12), the reflected waves were deviated from the incident direction at the lower workpiece and fixture surface (i.e., interface III), and consequently resulted in an ultrasonic energy deviation at the faying surface (i.e., interface II). Referring to Fig. 12, the angles of incidence are 0, 2θ, 4θ at interface I and θ, 3θ, 5θ at interface III in the first three cycles for the weld made with the horn misalignments, respectively. Furthermore, because the coefficient of friction and horn pressure at the horn to workpiece and workpiece to workpiece are similar (Refs. 25, 26), the absorption coefficient (i.e., α_1) of interface I is assumed to be the same as that of interface II (i.e., $\alpha_1=\alpha_2=\alpha$). The power of the weld machine (i.e., output energy per unit time) is defined as P, and S_i is the contact area between the horn and upper workpiece. Hence, the energy density (i.e., dissipated energy/unit area/unit time), E_0, can be expressed as follows:

$$E_0 = P/S_i \quad (1)$$

The energy density inducted into interfaces I, II, and III in the first cycle can be written as

$$E_1 = E_0T_1 \quad (2)$$

$$E_2 = E_0T_1e^{-2\lambda x} \quad (3)$$

$$E_3 = E_0T_1T_2e^{-4\lambda x} \quad (4)$$

where x is the thickness of the workpiece, T_1 and T_2 are the transmitted coefficients at interfaces I and II, respectively, λ is the damping factor on the amplitude of the ultrasonic welding machine, and $e^{-2\lambda x}$ is the damping factor (Ref. 18) of the weld energy in the upper workpiece. As shown in Fig. 12, the reflected energy at interface III is conducted into interfaces II and I again, and then, the energy density at interface II in the first cycle is

$$E_{2-fc} = E_0T_1\alpha(e^{-2\lambda x}+T_2\gamma_3e^{-6\lambda x}) \quad (5)$$

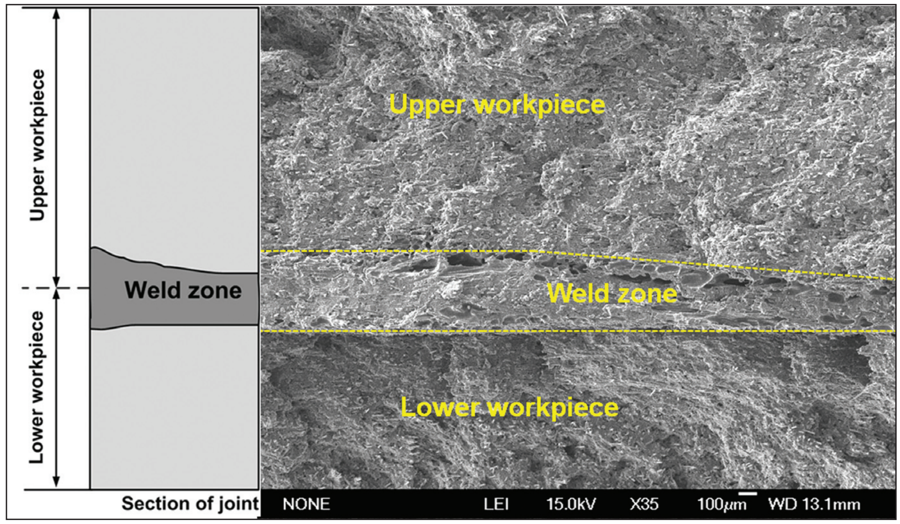

Fig. 8 — Microstructure at region 2 of ultrasonic welded C_f/PA 66 composite with a 4-deg horn axial misalignment.

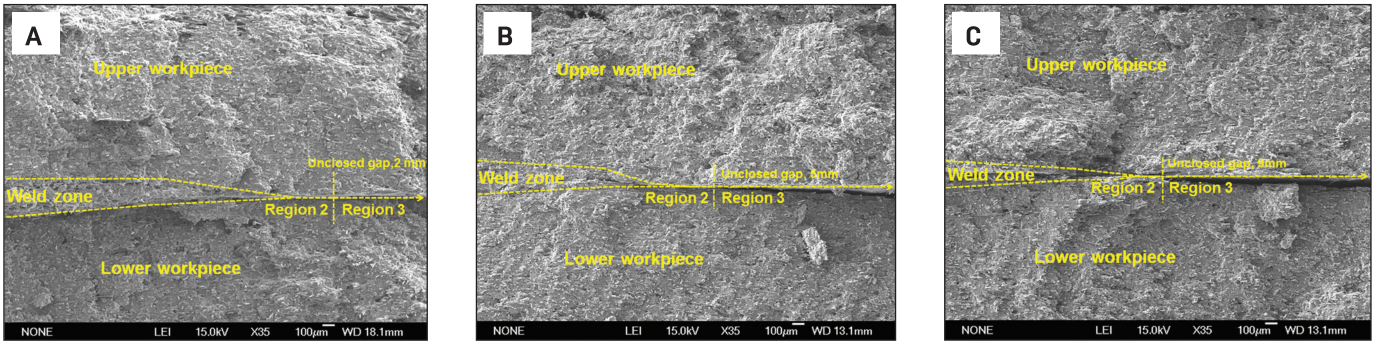

Fig. 9 — Effect of horn axial misalignment on the microstructures at region 3 of the ultrasonic welded C_f/PA 66 composite with 30 wt-% fiber: A — 2; B — 4; C — 6 deg.

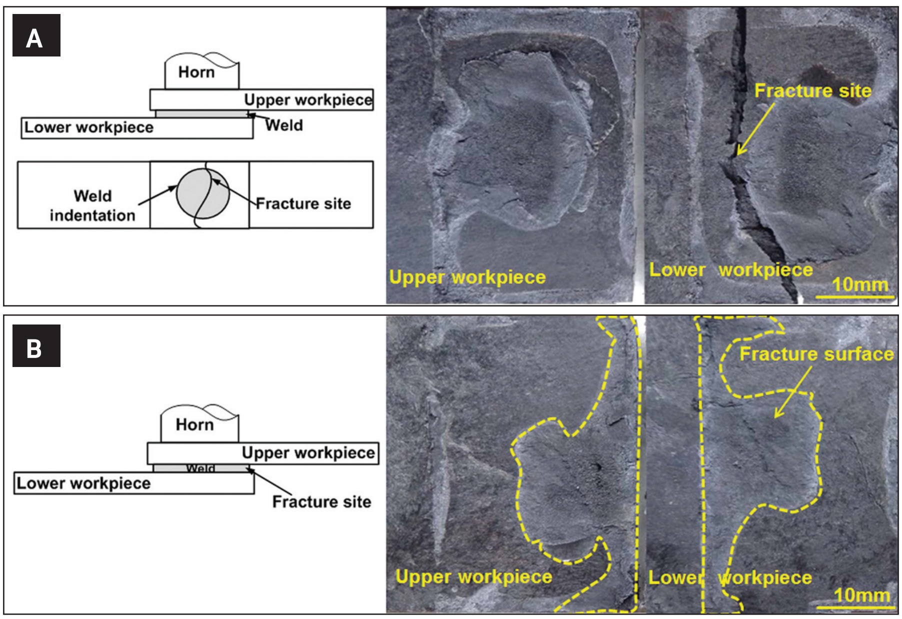

Fig. 10 — Effect of horn misalignment on the fracture mode for ultrasonic welded 4-mm- (0.16-in.-) thick C_f/PA 66 composite: A — 2; B — 6 deg.

After one cycle, the absorptivity of the weld energy at interface II can be expressed as

$$K=\frac{E_{2\text{-}fc}}{E_1}=\alpha\left[e^{-2\lambda x}+(1-a)g_3e^{-6lx}\right] \quad (6)$$

At the end of the first cycle, the returned energy density of ultrasonic waves at interface I (i.e., the energy for the second cycle) is

$$E_{1re} = E_0T_1e^{-8\lambda x}(1-\alpha)^2\gamma_3\gamma_1 \quad (7)$$

The ratio of returned energy density to the initial energy density at interface I (E_1), n, after one cycle and the energy density for the mth cycle, E_{dm}, at interface II during welding can be expressed in Equations 8 and 9, respectively,

$$n=\frac{E_{1re}}{E_1}=e^{-8\lambda x}(1-\alpha)^2\gamma_3\gamma_1 \quad (8)$$

$$E_{dm} = n^{m-1}KE_0(1-\gamma_1-\alpha) \quad (9)$$

where m is the number of the ultrasonic wave traveling cycle. γ_1 and γ_3 are the reflected coefficients at interfaces I and III, respectively, which can be estimated by Equations 10 and 11 (Ref. 27).

$$\gamma_1=\left(\frac{\rho_2c_2\cos\theta_i-\rho_1c_1\cos\theta_t}{\rho_2c_2\cos\theta_i+\rho_1c_1\cos\theta_t}\right)^2 \quad (10)$$

$$\gamma_3=\left(\frac{\rho_3c_3\cos\theta_i-\rho_2c_2\cos\theta_t}{\rho_3c_3\cos\theta_i+\rho_2c_2\cos\theta_t}\right)^2 \quad (11)$$

where ρ_1, ρ_2, and ρ_3 are the densities of the horn, C_f/PA 66 composite, and anvil, respectively; c_1, c_2, and c_3 are the sound velocities in the horn, C_f/PA 66 composite, and anvil, respectively; θ_i is the incident angle (i.e., a horn off-angle); and θ_t is the transmitted angle. The relationship between θ_i and θ_t angles can be described with Snell's law (Ref. 28). Since the coefficients of reflection (γ), transmission (T), and absorption (α) of a wave satisfy the equation $\gamma + T + \alpha = 1$ at each interface (Ref. 29), the absorption coefficient α at interface II was estimated with the use of Equations 8 and 9.

Table 1 — Effect of Horn Axial Misalignment on the Reflection Coefficients at Interfaces I and III

Horn misalignment (degree)	Reflection coefficient (γ_1)			Reflection coefficient (γ_3)		
	First cycle	Second cycle	Third cycle	First cycle	Second cycle	Third cycle
0	0.383	0.383	0.383	0.732	0.732	0.732
2	0.383	0.386	0.394	0.733	0.736	0.774
4	0.383	0.394	0.432	0.734	0.748	0.785
6	0.383	0.409	0.526	0.736	0.774	—

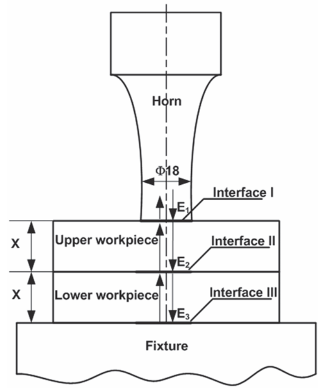

Fig. 11 — Schematic of the ultrasonic welding process without a horn misalignment (Ref. 20).

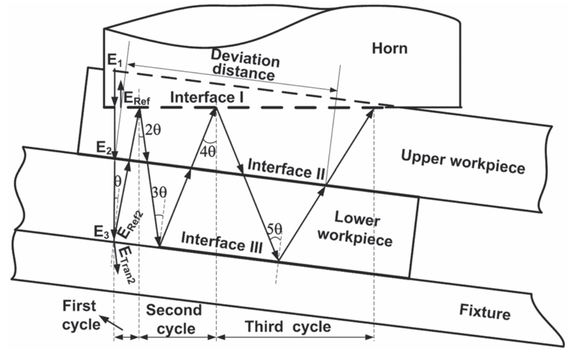

Fig. 12 — Schematic of the effect of horn misalignment on ultrasonic wave traveling in ultrasonic welding.

Based on the model shown in Fig. 12, the reflected waves are deviated from the incident directions, and thus the decrease in weld area and weld strength with an increase in horn misalignment, shown in Fig. 4, was likely related to the energy deviation at interface II. These results indicate the weld size was related to not only the absorption coefficient (α) but also the dissipated energy at interface II.

During ultrasonic wave propagation, the energy density would accumulate and overlap at the faying interface II resulting from a horn misalignment. If ultrasonic waves are reflected at interfaces I and III and propagated along the Y direction for the joint with a horn misalignment, the ultrasonic wave would transmit through interface II and the energy from the reflected waves would be absorbed and accumulated at interface II, as shown in Fig. 13. Referring to Fig. 13A, the red area represents ultrasonic waves propagating from interface I to interface III, and the blue area illustrates the waves reflected to interface I from interface III. The green area shows the waves reflected to interface III from interface I again. The presence of the horn misalignment results in the overlap of the red, blue, and green areas as shown in Fig. 13B. Because ultrasonic waves travel from interface I to interface III (and vice versa), part of the ultrasonic energy is absorbed by interface II, and hence the energy density at interface II is accumulated as shown in Fig. 13C.

The relation between the required time for melting the material and energy density (E_d) during ultrasonic welding can also be expressed as Equation 12 (Ref. 30):

$$t_m = \frac{\pi}{a}\left[\frac{k^2\theta_m^2}{E_d^2}\right] \qquad (12)$$

where a is the thermal diffusivity of the workpiece, k is the thermal conductivity, θ_m is the difference between ambient and melting temperatures, and t_m is the required time for interface II to reach the melting temperature of the workpieces. Then, Equation 12 can be rewritten as

$$t_m E_d^2 = \pi K^2 \theta_m^2 / a \qquad (13)$$

The right side of Equation 13 is related to the intrinsic material properties, while the left side is related to the process parameters of the ultrasonic welding process. Examination of Equation 13 indicated the melting of materials at the faying surfaces was determined by the value of $\pi K^2\theta_m^2/a$ despite the welding conditions, suggesting the value of $\pi K^2\theta_m^2/a$ was the threshold for melting materials at the faying surfaces. To melt the material and form a weld, the value of tE_d^2 (where t is the weld time) must be greater than the threshold.

Figure 13C shows the values of E_d varied along the Y direction at the faying surfaces for the joint with a horn misalignment. Based on the above discussion, the materials would be melted and a weld would be formed when tE_d^2 at a specific Y position is greater than the threshold value ($\pi K^2\theta_m^2/a$). The size of the weld was determined by comparing the value of tE_d^2 at any Y position at the faying surfaces to the value of $\pi K^2\theta_m^2/a$, referring to Fig. 13D. With the procedure described above, the effect of horn misalignment on the weld size was established.

Estimation of Weld Size

Based on the model described above, the effect of horn misalignment on the weld size in ultrasonic welding of C_f/PA 66 composite was examined. By plugging the densities of the horn, C_f/PA 66 composite and anvil [i.e., 2.81, 1.22, and 7.85 g/cm^3 (Ref. 31), respectively], sound velocities in the horn, C_f/PA 66 composite and anvil [i.e., 5000, 2591, and 5200 m/s (Ref. 32), respectively] into Equations 10 and 11, the reflection coefficients (i.e., γ_1 and γ_3) were estimated and the results are shown in Table 1. Referring to Table 1, the estimated reflection coefficients γ_1 and γ_3 at the interfaces increased slightly with an increase in horn axial misalignment.

Because the absorption coefficient α at interface II of C_f/PA 66 composite was hardly influenced by the horn misalignment, it can be estimated with Equations 8 and 9. For the joint without a horn misalignment, the dissipated energy density at interface II was obtained by the accumulation of E_{dm} as shown in Fig. 13C. The relation between the energy density (E_{dm}) and total dissipated energy per unit time (P_d) at the faying surfaces can be expressed as

$$P_d = E_d S_i = \Sigma E_{dm} S_i \qquad (14)$$

In fact, the dissipated energy, P_d, for melting the materials at the faying

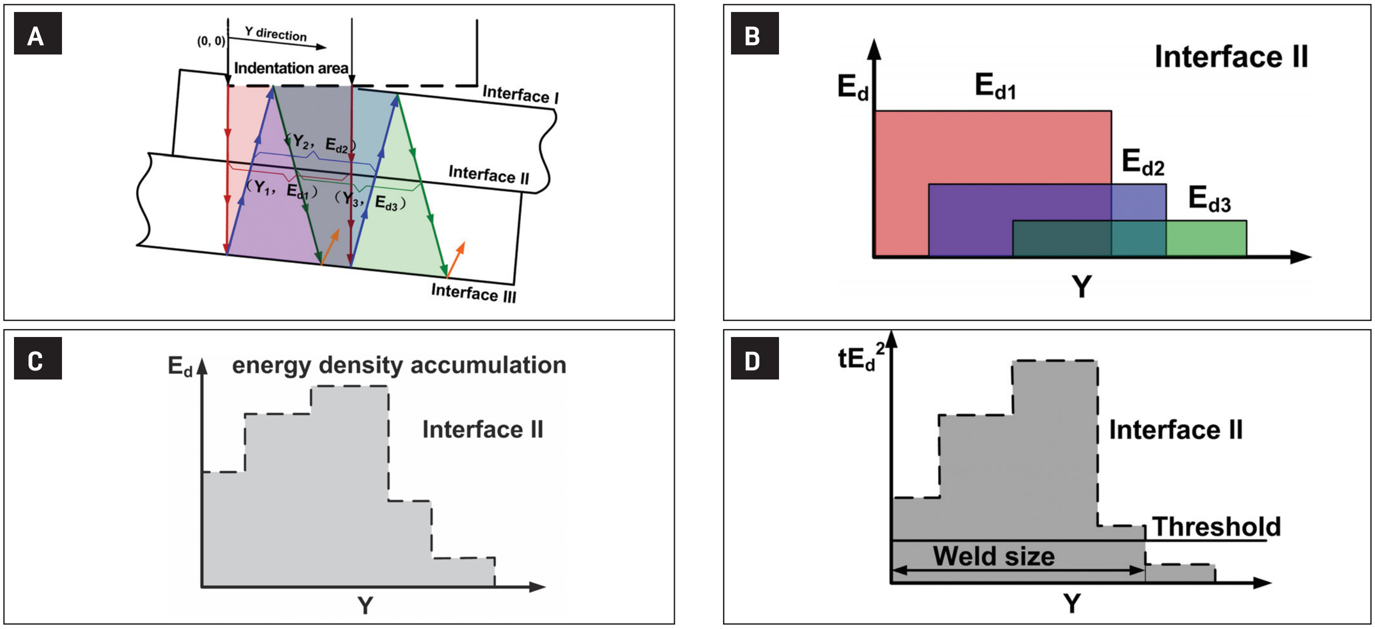

Fig. 13 — Model for ultrasonic waves traveling in a lapped joint with the following: A — A horn misalignment; B — reflection of energy density; C — accumulation of energy density; and D — estimation of the weld size.

surfaces in phase I during ultrasonic welding, can be estimated with Equations 9 and 12 (Ref. 30). For the joint made without a horn misalignment, S_i is the face area of the horn (i.e., $2.54 \times 10^{-4} m^2$), t_m is 0.3 s (obtained from Ref. 33). By plugging the values of $a = 8.7 \times 10^{-3} cm^2/s$, $k = 1.5$ W/m·K, and θ_m = 240k (Ref. 34) into Equations 12 and 14, the dissipated energy per unit time ($P_d = 290.8$ J·s^{-1}) and energy density (E_d) at interface II with a horn inclination of 0 deg ($E_{d-0} = 1.15 \times 10^6$ J·m^{-2}·s^{-1}) were estimated.

Having substituted the values of λ (0.37, damping factor on the amplitude of the ultrasonic welding machine) (Ref. 22), γ_1 and γ_3 (i.e., reflection coefficients shown in Table 1) into Equation 7, the ratios of the returned energy density to the initial energy density (n_1) were estimated as $0.277(1 - \alpha)^2$ for the first cycle. Because the returned energy of the ultrasonic waves at interface I at the end of the previous cycle is the energy for the following cycle, the ratios of the returned energy density to the initial energy density after m cycles can be expressed as n^{m-1}. With this derivation, the ratios of the returned energy density to the initial energy density were estimated and were about 27.7, 7.7, 2.1, and 0.5% of the initial ultrasonic energy density after one, two, three, and four cycles, respectively. These results indicated the weld energy was dissipated significantly after three cycles, and therefore only the first three cycles of ultrasonic wave propagation were considered for the rest of this study. The energy absorption coefficient ($\alpha = 0.16$) was obtained by substituting the number of the ultrasonic traveling cycles (m = 3), the dissipated energy per unit time at interface II for the first three cycles ($P_d = 290.8$ J·s^{-1}), and the energy per unit time inducted into the materials from the welding horn ($P_0 = 2000$ J·s^{-1}) into Equations 9 and 14 (Ref. 31). Then, the effect of horn misalignment on the dissipated energy per unit time (P_m) at the faying surfaces (i.e., interface II) after each cycle was estimated using Equation 14 and the results are listed in Table 2. As shown, the horn misalignment slightly influenced the total dissipated energy per unit time at the faying surfaces during the welding process. It was inferred that the weld size was influenced by the energy density (E_d) rather than the dissipated energy at interface II.

To estimate the dissipated energy density (E_d), the deviation distances after each propagated cycle resulting from the horn misalignment were estimated per the geometrical relationship between the thickness of the workpiece and angles of incidence (θ) shown in Fig. 12. Table 3 lists the effect of horn misalignment on the deviation distance and weld size. As shown, the deviation distance at interface II caused by the horn misalignment increased with an increase in horn misalignment, which was pronounced for a 6-deg horn misalignment. These results implied that the deviation of the ultrasonic wave led to the dispersion of the weld energy at interface II (i.e., faying surfaces).

To estimate the influence of horn misalignment on the weld size, the values of tE_d^2 for the welds with various horn misalignments were estimated using Equation 9 and accumulated per the model in Fig. 13D. By plugging the values of a, k, and θ_m (Ref. 32) into $\pi K^2\theta_m^2/a$, the threshold value ($\pi K^2\theta_m^2/a$) to form a weld at the faying surfaces was 4.68×10^{11} (J/m^2)^2·s^{-1}. Once the value of tE_d^2 at any Y position at the faying surfaces exceeded the threshold, the material started to melt and formed a weld with a size Y. Figure 14 presents the estimated values of tE_d^2 as a function of Y for the joints with various horn misalignments. The estimated weld sizes were 18, 13, and 11 mm (0.71, 0.51, and 0.43 in.) and 10 mm (0.39 in.) for the 0-, 2-, 4-, and 6-deg horn misalignment, respectively. To validate the modeling results, measured and estimated weld sizes were compared and the results are shown in Fig. 15. As shown, the estimated weld sizes were smaller than the measured weld sizes, which was likely attributed to the fact the flow of the molten material at interface II was not considered in the modeling.

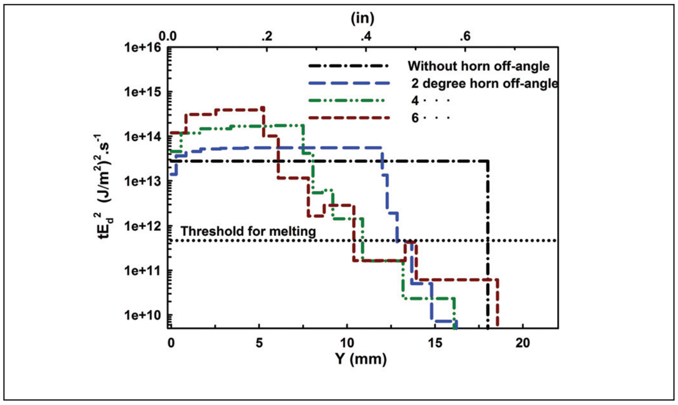

Fig. 14 — Estimation of weld size at interface II (i.e., faying surface) in ultrasonic welding of 4-mm- (0.16-in.-) thick C_f/PA 66 composite with 30 wt-% fiber.

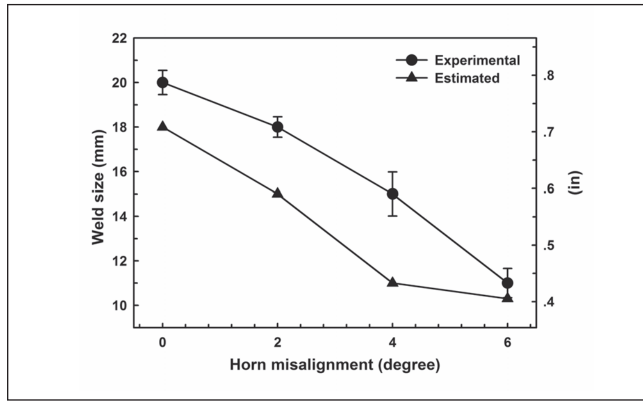

Fig. 15 — Comparison of the measured and estimated weld sizes in ultrasonic welding of 4-mm- (0.16-in.-) thick C_f/PA 66 composite with 30 wt-% fiber.

Summary

It is emphasized that the results presented in this study only illustrate the reduction of quasi-static strength of ultrasonic welded 4 mm (0.16 in.) carbon-fiber polyamide 66 composite with 30% mass made with 2- to 6-deg horn misalignment. The horn misalignment and tooling (i.e., horn and fixture) reported here are not indicative of the specific environment and tooling encountered by the manufacturing production. Nevertheless, the present results show reduction of static strengths due to horn misalignment needs to be considered during the structural design. Therefore, it is recommended that proper joint strengths used in structural design be considered and adjusted to account for likely horn misalignment.

Conclusions

It is important to note that the analytical model developed herein is a first-level approach to understand the trends in weld size as affected by horn misalignment. It is most interesting that the experimental results support the estimates derived from the analytical model, despite the model not incorporating the flow of the molten material at the faying surfaces and part fitup (i.e., gap between the workpieces). The use of the model would increase the design and manufacturing flexibility of the ultrasonic weld assembly. Investigation of the influence of horn misalignment on the weld quality in ultrasonic welding of 4-mm- (0.16-in.-) thick C_f/PA 66 composite with 30 wt-% fiber by both modeling and experimental testing led to the following conclusions:

1. An analytical model was derived to estimate the energy absorption in the welding zone of the thermoplastic material, and consequently permits the estimation of weld size.

2. Horn-to-workpiece axial alignment angle beyond 4 deg resulted in a significant decrease in weld area, weld strength, and cosmetic quality.

3. The presence of the horn axial misalignment resulted in the reflected wave deviating from the incident direction and the energy deviation at the faying surfaces, and consequently led to a discrepant weld.

Acknowledgments

The authors gratefully acknowledge the financial and technical support provided by GM Global Research and Development Center to carry out the present work.

Table 2 — Effect of Horn Axial Misalignment on the Estimated Energy Dissipated at Interface II

Horn misalignment, (degree)	Energy absorption, P_m, (J•s⁻¹) First cycle	Second cycle	Third cycle	Total energy absorption P_d, (J•s⁻¹)
0	237.0	45.0	8.8	290.8
2	237.5	45.9	8.9	292.3
4	237.6	46.2	9.1	292.9
6	237.8	46.8	10.1	294.7

Table 3 — Effect of Horn Misalignment on the Deviation Distance and Weld Size at Interface II

Horn misalignment (degree)	Deviation distance (mm) First cycle	Second cycle	Third cycle	Total deviation distance (mm)	Measured weld size (mm)	Contact area (mm²)
0	0	0	0	0	20	254.3
2	0.28	1.4	2.53	4.21	18	189.1
4	0.56	2.82	5.2	8.59	15	105.0
6	0.84	4.3	8.2	13.3	11	66

References

1. Kim, Y. K., Kwon, H. Choi, W. J., Woo, C. S., and Park, H. S. 2011. Environmental considerations of plastic behaviors for automobile applications. *Procedia Engineering* 10: 1029–1034. DOI: 10.1016/j.proeng.2011.04.169.

2. Gutnik, V. G., Gorbach, N. V., and Dashkov, A. V. 2002. Some characteristics of ultrasonic welding of polymers. *Fibre Chemistry* 34: 426–432. DOI: 10.1023/A:1022912325343.

3. Kiziltas, A., Gardner, D. J., Han, Y., and Yang, H.-S. 2014. Mechanical properties of microcrystalline cellulose (MCC) filled engineering thermoplastic composites. *Journal of Polymer & the Environment* 22: 365–372. DOI: 10.1007/s10924-014-0676-5.

4. Jia, N., and Fraenkel, H. A. 2004. Effects of moisture conditioning methods on mechanical properties of injection molded Nylon 6. *Journal of Reinforced Plastic and Composite* 23: 729–737. DOI: 10.1177/0731684404030730.

5. Mubashir, S., and Muttana, S. B. 2012. Carbon fibre composites: Outlook for the automobile sector. *Auto Tech Review* 1: 18–23. DOI: 10.1365/s40112-012-0075-z.

6. Zhang, G., Qiu, J., Shao, L., Liu, M., Zhang, M., and Wu, Y. 2011. Ultrasonic weld properties of heterogeneous polymers: Polylactide and poly (methyl methacrylate). *Journal of Materials Processing Technology* 211: 1358–1363. DOI: 10.1016/j.jmatprotec.2011.03.005.

7. Cosson, B., Deléglise, M., and Knapp, W. 2015. Numerical analysis of thermoplastic composites laser welding using ray tracing method. *Composites: Part B* 68: 85–91. DOI: 10.1016/j.compositesb.2014.08.028.

8. Amanat, N., James, N. L., and McKenzie, D. R. Welding methods for joining thermoplastic polymers for the hermetic enclosure of medical devices. *Medical Engineering & Physics* 32: 690–699. DOI: 10.1016/j.medengphy.2010.04.011.

9. da Costa, A. P., Botelho, E. C., Costa, M. L., Narita, N. E., and Tarpani, J. R. 2012. A review of welding technologies for thermoplastic composites in aerospace applications. *Journal of Aerospace Technology & Management* 4: 255–265. DOI: 10.5028/jatm.2012.04033912.

10. Ageorges, C., Ye, L., and Hou, M. Advances in fusion bonding techniques for joining thermoplastic matrix composites: A review. *Composites: Part A* 32: 839–857. DOI: 10.1016/S1359-835X(00)00166-4.

11. Sackmann, J., Burlage, K., Gerhardy, C., Memering, B., Liao, S., and Schomburg, W. K. 2014. Review on ultrasonic fabrication of polymer micro devices. *Ultrasonics* 56: 189–200. DOI: 10.1016/j.ultras.2014.08.007.

12. Van Wijk, H., Luiten, G. A., Van Engen, P. G., and Nonhof, N. J. 2010. Process optimization of ultrasonic welding. *Polymer Engineering and Science* 36: 1165–1176. DOI: 10.1002/pen.10510.

13. Potente, H. 1984. Ultrasonic welding — Principles & theory. *Materials & Design* 5: 228–234. DOI: 10.1016/ 0261-3069(84)90032-3.

14. Sahin, O. S., Koellhoffer, S., Gillespie, J., Advani, S., and Bogetti, T. 2014. Thermal modeling during continuous ultrasonic welding. *Turkish Journal of Engineering & Sciences* 38: 79–96. DOI: 10.3906/muh-1402-13.

15. Siddiq, A., and Ghassemieh, E. 2008. Thermomechanical analyses of ultrasonic welding process using thermal and acoustic softening effects. *Mechanics of Materials* 40: 982–1000. DOI: 10.1016/j.mechmat.2008.06.004.

16. Lazri, H., Ogam, E., Amar, B., Fellah, Z. E. A., Oduor, A. O., and Baki, P. 2017. Identification of the mechanical moduli of flexible thermoplastic thin films using reflected ultrasonic waves: Inverse problem. *Ultrasonics* 81: 10–22. DOI: 10.1016/j.ultras.2017.05.011.

17. Merdjana, H., Boukabou, A., and Grimes, M. 2018. A high accuracy ultrasonic measurement system using the prism technique. *Measurement* 114: 195–202. DOI: 10.1016/j.measurement. 2017.09.042.

18. Khmelev, V. N., Slivin, A. N., and Abramov, A. D. 2007. Model of process and calculation of energy for a heat generation of a welded joint at ultrasonic welding polymeric thermoplastic materials. *8th Siberian Russian Workshop and Tutorial on Electron Devices and Materials*, pp. 316–322. DOI: 10.1109/SIBEDM.2007. 4292995.

19. Rani, R. M., Suresh, K. S., Prakasan, K., and Rudramoorthy, R. 2007. A statistical study of parameters in ultrasonic welding of plastics. *Experimental Techniques* 31: 53–58. DOI: 10.1111/j1747-1567.2007.00182.x.

20. Balkan, O., Demirer, H., and Yildirim, H. 2008. Morphological and mechanical properties of hot gas welded PE, PP and PVC sheets. *Journal of Achievements in Materials and Manufacturing Engineering* 31: 60–70. DOI: 10.1002/ pen.21014.

21. Von White II, G., Smith, J. N., Clough, R. L., Ohlhausen, J. A., Hochrein, J. M., and Bernstein, R. 2012. The origins of CO_2 and NH_3 in the thermal-oxidative degradation of Nylon 6.6. *Polymer Degradation and Stability* 97: 1396–1404. DOI: 10.1016/j.polymdegradstab.2012. 05.018.

22. Zhi, Q., Tan, X., and Liu, Z.-X. 2017. Effect of moisture on the ultrasonic welding of carbon-fiber reinforced Nylon 66 composite. *Welding Journal* 96(6): 185-s to 192-s.

23. Zhi, Q., Tan, X., Lu, L. Chen, L., Li, J., and Liu, Z.-X. 2017. Decomposition of ultrasonically welded carbon fiber/polyamide 66 and its effect on weld quality. *Welding in the World* 61: 1017–1028. DOI: 10.1007/s40194-017-0482-5.

24. Weglowskan, A., and Pietras, A. 2012. Influence of the welding parameters on the structure and mechanical properties of vibration welded joints of dissimilar grades of nylons. *Archives of Civil and Mechanical Engineering* 12: 198–204. DOI: 10.1016/j.acme.2012.03.009.

25. Benatar, A., Eswaran, R. V., and Nayar, S. K. 1989. Ultrasonic welding of thermoplastics in the near-field. *Polymer Engineering and Science* 29: 1689–1698. DOI: 10.1002/pen.760292311.

26. Tolunay, M. N., Dawson, P. R., and Wang, K. K. 1983. Heating and bonding mechanisms in ultrasonic welding of thermoplastics. *Polymer Engineering and Science* 23: 726–733. DOI: 10.1002/ pen.760231307.

27. Zhu, R., Liu, X. N., and Huang, G. L. 2015. Study of anomalous wave propagation and reflection in semi-infinite elastic metamaterials. *Wave Motion* 55: 73–83. DOI: 10.1016/j.wavemoti.2014.12.007.

28. Cap, N., Ruiz, B., and Rabal, H. 2003. Refraction holodiagrams and Snell's law. *Optik* 114(2): 89–94. DOI: 10.1078/0030-4026-00227.

29. Castagnede, B., Saeid, M., Moussatov, A., Gusev, V., and Tournat, V. 2006. Reflection and transmission at normal incidence onto air-saturated porous materials and direct measurements based on parametric demodulated ultrasonic waves. *Ultrasonics* 44: 221–229. DOI: 10.1016/j.ultras.2005.11.004.

30. Stokes, V. K. 1988. Vibration welding of thermoplastics, Part II: Analysis of the welding process. *Polymer Engineering and Science* 28(1988): 728–739. DOI: 10.1002/pen.760281105.

31. Web Elements: *webelements.com/periodicity/density*.

32. *webelements.com/periodicity/velocity_sound*.

33. Zhi, Q., Lu, L., Gao, Y.-H., Liu, Z.-X., and Wang, P.-C. 2018. Online weld quality inspection in ultrasonic welding carbon fiber/PA 66 composites without energy director. *Welding Journal* 97(3): 65-s to 74-s. DOI: 10.29391/2018.97.006.

34. *funnelweb.utcc.utk.edu/～athas/databank/intro.html*.

QIAN ZHI, LEI LU, and ZHONG-XIA LIU (zzuliuzhongxia6@163.com) are with Key Lab of Materials Physics, School of Physics and Engineering, Zhengzhou University, Zhengzhou, Henan, China. PEI-CHUNG WANG is with Manufacturing Systems Research Lab, General Motors Global Research and Development Center, Warren, Mich.